Journal of Applied Polymer Science

Statistical Characterization of the Impact Strengths of Vapor-Grown Carbon Nanofiber/Vinyl Ester Nanocomposites Using a Central Composite Design

Glenn W. Torres,[1] Sasan Nouranian,[2,3] Thomas E. Lacy,[1] Hossein Toghiani,[2] Charles U. Pittman Jr.,[4] Janice L. DuBien[5]

[1]Department of Aerospace Engineering, Mississippi State University, Mississippi State, Mississippi 39762
[2]The Dave C. Swalm School of Chemical Engineering, Mississippi State University, Mississippi State, Mississippi 39762
[3]Center for Advanced Vehicular Systems (CAVS), Mississippi State, Mississippi 39762-5405
[4]Department of Chemistry, Mississippi State University, Mississippi State, Mississippi 39762
[5]Department of Mathematics and Statistics, Mississippi State University, Mississippi 39762
Correspondence to: T. E. Lacy (E-mail: lacy@ae.msstate.edu)

ABSTRACT: The effects of vapor-grown carbon nanofiber (VGCNF) weight fraction, high-shear mixing time, and ultrasonication time on the Izod impact strengths of VGCNF/vinyl ester (VE) nanocomposites were studied using a central composite design. A response surface model (RSM) for predicting impact strengths was developed using regression analysis. RSM predictions suggested that an 18% increase in impact strength was possible for nanocomposites containing only 0.170 parts per hundred parts resin (phr) of VGCNFs (~0.1 v%) that were high-shear mixed for 100 min when compared to that of neat VE. In general, the predicted impact strengths increased for high-shear mixing times above 55 min and VGCNF weight fractions below 0.400 phr. The predicted strengths decreased as the VGCNF weight fraction was further increased. Scanning electron micrographs of the nanocomposite fracture surfaces showed that increased impact strength could be directly correlated to better nanofiber dispersion in the matrix.
 J. Appl. Polym. Sci. 000: 000–000, 2012

KEYWORDS: carbon nanofibers; vinyl ester; thermosets; nanocomposites; impact resistance

Received 20 March 2012; accepted 12 June 2012; published online
DOI: 10.1002/app.38190

INTRODUCTION

Polymer nanocomposites hold the promise of increased mechanical,[1] thermal,[2,3] and electrical properties[4] relative to traditional structural materials. Relatively large nanofiller surface-area-to-volume ratios can produce increased shear load transfer from the polymer matrix to the nanoreinforcements, often resulting in increased mechanical properties at low reinforcement amounts (~1–2 v%) relative to the neat polymer.[5] Nanoreinforcements are defined as having at least one dimension on the nanoscale and typically come in the form of platelets, spheres, fibers, or tubes/rods.[1,6]

Vapor-grown carbon nanofibers (VGCNFs) have recently received much attention because of their comparatively low cost and good mechanical, thermal, and electrical properties.[7] VGCNFs typically have hollow cylindrical cross-sections with average diameters, $D = 120$ nm, and aspect ratios, $L/D = 50$–$2000+$.[8] The mechanical properties of VGCNF-reinforced nanocomposites and VGCNF-enhanced fiber composites are highly dependent on nanofiber dispersion within the matrix.[9–13] Agglomerates, or bird's-nest-like entanglements of undispersed nanofiber bundles, are formed due to strong van der Waals forces between nanofibers as well as their wavy shapes. Poor nanocomposite mechanical characteristics result from nanofiber agglomeration and the localized stress concentrations that form at such inhomogeneities.[14] Recent efforts to minimize agglomerates tend to use a combination of nanofiber surface treatments and mixing techniques.[15–17]

Vinyl ester (VE) is a cost-effective thermosetting resin with mechanical and chemical properties suitable for reinforcement with VGCNFs. It was used as the matrix with VGCNFs in our earlier studies.[8,10–12,18,19] Lee[12] performed quasi-static flexure and tensile tests on VGCNF/VE nanocomposites. Nanocomposites prepared with surface-oxidized VGCNFs and a dispersing agent improved the nanocomposite flexural properties over those containing unoxidized VGCNFs with no dispersing agent.

A major concern when using nanocomposites in structural applications, such as load bearing automotive and aerospace

parts, is to understand the effect of nanoreinforcements on impact properties. Fidelus et al.[20] studied the impact strengths of an epoxy resin reinforced with single- and multi-wall carbon nanotubes (CNTs). At extremely low CNT weight fractions [<0.05 parts per hundred parts resin (phr) by weight], composite impact strengths exceeded that of the neat epoxy resin. Similar tests by Miyagawa and Drzal[21] exhibited no improvement in nanocomposite impact strengths with the addition of up to 0.3 wt % of CNTs. The impact strengths began to deteriorate with further CNT addition.

In this work, Izod impact tests were performed on VGCNF/VE nanocomposites prepared using oxidized VGCNFs and a dispersing agent. A response surface methodology[22] was employed in a central composite design (CCD)[23,24] in order to isolate and examine the effects of multiple factors (i.e., VGCNF weight fraction, high-shear mixing time, and ultrasonication time) on nanocomposite impact strengths using the minimum number of runs. In the context of polymer composites, such powerful statistical techniques have previously been used for dynamic mechanical analysis of VGCNF/VE nanocomposites,[10] damage characterization of sandwich composites,[25–28] epoxy nanocomposites,[29] thermoplastic starch/clay nanocomposites,[30] polyurethane/clay nanocomposites,[31] polystyrene/montmorillonite nanocomposites,[32] and so forth. High-shear mixing and ultrasonication were chosen as the mixing techniques due to their prevalent use in previous studies.[10,12,15–17] The VGCNF/VE resin system considered in this study can potentially be used in conjunction with traditional continuous fiber reinforcements. One long-term goal of this work is to develop E-glass/VGCNF/VE hybrid composites for primary automotive structural applications, with a focus on crash and energy absorbing structures. Hence, understanding the impact strength of the nanophased matrix is of paramount importance.

EXPERIMENTAL

Design of Experiments

A three-factor CCD[23,24] was employed to determine the effects of VGCNF weight fraction (X_1), high-shear mixing time (X_2), and ultrasonication time (X_3) on the impact strengths of VGCNF/VE nanocomposites. The CCD consisted of 15 design points, including eight factorial ("corner") points based on a 2^3 factorial design, one center point, and six axial ("star") points at a normalized distance $\alpha = \sqrt{2}$ from the center point. In addition, four runs at the design center point were used to estimate the pure error, resulting in a total of 18 experimental runs. The CCD is a very flexible and efficient design for fitting a full quadratic response surface model (RSM). Here, it is assumed that the response (i.e., impact strength) contains a certain degree of quadratic curvature associated with each factor, as well as curvature due to pairwise interactions between factors. The 18 runs may be used to estimate the 10 parameters in the full quadratic RSM. The remaining degrees of freedom may be used to test for lack of fit or add higher order terms to the RSM if warranted.

The range of design levels for each independent variable in the current work was determined based on a series of previous studies.[10,12] The VGCNF weight fraction (X_1) ranged from $X_1 =$ 0.176−1.024 phr. In this study, it was assumed that the presence of nanofibers in such small amounts had a negligible effect on the degree of resin curing. The upper limit of VGCNF weight fraction ($X_1 = 1.024$ phr) was dictated by the increasing viscosity of the uncured VGCNF/resin mixture associated with increasing VGCNF weight fraction.[33] At VGCNF weight fractions exceeding 1.000 phr, the increased VGCNF/resin mixture viscosity prohibited effective nanofiber dispersion. The lower limit of VGCNF weight fraction ($X_1 = 0.176$ phr) was set so that there would be enough carbon nanofibers present to have an effect on the impact properties of the nanocomposites.

Table I. Coded and Uncoded Values for the Central Composite Design Test Matrix

x_i	X_1 (phr[a])	X_2 (min)	X_3 (min)
$-\sqrt{2}$	0.176	0.00	0.00
−1	0.300	14.64	8.79
0	0.600	50.00	30.00
1	0.900	85.36	51.21
$\sqrt{2}$	1.024	100.00	60.00

[a]Parts per hundred parts resin.

The high-shear mixing time (X_2) ranged from $X_2 = 0-100$ min. The upper limit for high-shear mixing time was set at $X_2 = 100$ min to avoid significant styrene evaporation with increased mixing time. Styrene is a comonomer present in the VE resin. The cured matrix would become more brittle due to higher crosslink densities if significant amounts of styrene were lost. The specified upper limit also decreased the risk of severely chopping the nanofibers with excessive high-shear mixing. Nanofiber breakage reduces the nanofiber aspect ratio and negatively affects the nanocomposite mechanical properties. The ultrasonication time (X_3) ranged from $X_3 = 0-60$ min. The upper ultrasonication time limit was set at $X_3 = 60$ min to avoid the risk of excessive heating near the ultrasonic tip, as well as the risk of nanofiber damage and styrene evaporation at extended ultrasonication times. Excessive high-shear mixing and the tip heating can both cause significant styrene evaporation, which in turn can alter the curing chemistry.

Development of the design space using a CCD requires that the independent factor levels (X_i) are transformed into nondimensional ("coded") levels (i.e., $x_i = -\sqrt{2}$, -1, 0, 1, $\sqrt{2}$). Here, selection of the star points, $x_i = \pm\sqrt{2}$, corresponds to an orthogonal experimental design.[23,24] This suggests that the parameter estimates obtained in the RSM are independent. Table I relates the coded level (x_i) for each independent factor to its corresponding actual ("uncoded") value (X_i). The coded levels of a given independent variable may be expressed in terms of the uncoded values, that is,

$$x_i = \frac{2X_i - (X_{\text{iHigh}} + X_{\text{iLow}})}{X_{\text{iHigh}} - X_{\text{iLow}}}, \quad (1)$$

where, X_{iLow} and X_{iHigh} are chosen values corresponding to $x_i = -1$ and 1, respectively.

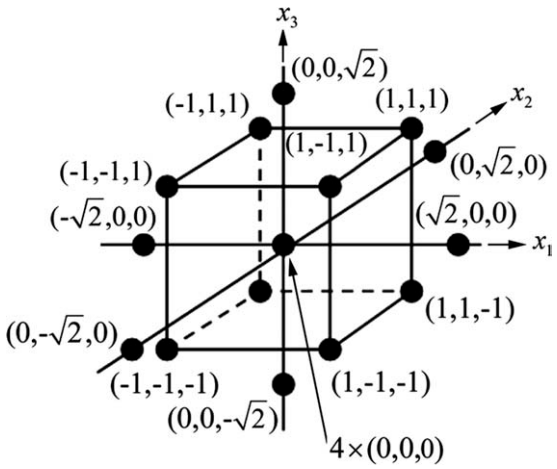

Figure 1. Graphical representation of a three-factor central composite design (Adapted from Ref. 22).

The CCD is graphically represented as a cube in the space of coded variables as shown in Figure 1.[23] Each node in the figure corresponds to a design point in the CCD. Table II presents each experimental run in its coded form along with its corresponding average measured Izod impact strength. For comparison, the average measured impact strength (S) for each experimental run was normalized with respect to the average measured impact strength of the neat VE (S_{VE} = 17.142 J/m). Also, the number of sample tests conducted for each experimental run (Freq.) and the standard deviation of the impact strength results for each experimental run (Std. Dev.) are presented in Table II. Experimental runs 2–5 and 10–13 ($x_1 = \pm 1$, $x_2 = \pm 1$, $x_3 = \pm 1$) correspond to the factorial (corner) design points of the cube. Experimental runs 15–18 ($x_1 = x_2 = x_3 = 0$) correspond to repeat runs at the center point of the design space. Experimental runs 1, 6–9, and 14 ($x_i = \pm\sqrt{2}$, $x_{i \neq j} = 0$) correspond to the axial design points.

The impact strengths corresponding to specific combinations of coded independent variables can be used to fit an RSM. This study uses a full quadratic RSM of the form

$$\frac{S}{S_{VE}} = \beta_0 + \sum_{i=1}^{k} \beta_i x_i + \sum_{i=1}^{k} \sum_{j=1}^{k} \beta_{ij} x_i x_j + \varepsilon \qquad (2)$$

where the normalized impact strength (S/S_{VE}) is the response of interest; the x_i's are independent variables [i.e., VGCNF weight fraction (x_1), high-shear mixing time (x_2), and ultrasonication time (x_3)]; β_0, β_i's, and β_{ij}'s are the unknown regression parameters; and $k = 3$ is the number of independent variables. The random error term ε, is assumed to have a normal distribution with a mean of zero and constant variance, which is typical in statistical modeling.

The unknown regression parameters can be estimated by the least squares method.[34] The RSM may be expressed in terms of the parameter estimates as

$$\frac{\hat{S}}{S_{VE}} = b_0 + \sum_{i=1}^{k} b_i x_i + \sum_{i=1}^{k} \sum_{j=1}^{k} b_{ij} x_i x_j \qquad (3)$$

where the caret (^) indicates that the predicted response is an estimate based upon the fitted RSM.

Materials

The VE resin chosen for this study, Derakane 441-400 (33 wt % styrene; Ashland, Inc., Covington, KY), was reinforced with surface-oxidized high temperature-pyrolyzed VGCNFs (PR-24-XT-LHT-OX, Applied Sciences, Inc., Cedarville, OH). Also included in the precured mixture were a catalyst promoter (6 wt % cobalt naphthenate in styrene, North American Composites Co., Lino Lakes, MN), two air release agents (BYK-A 515 and BYK-A 555, BYK USA, Inc., Wallingford, CT), a dispersing agent (BYK-9076, BYK USA, Inc., Wallingford, CT) and a free radical polymerization initiator [methyl ethyl ketone peroxide (MEKP), U.S. Composites, Inc., West Palm Beach, FL]. All of these components were mixed into a batch of 125 g of resin. Table III summarizes the precured composite mixture for 100 g of resin, which gives each of the nonresin components in phr.

Specimen Formulation

The first four ingredients in Table III were combined in order in a 240 mL container and hand-stirred until the resin had a uniform color. Impact specimens were fabricated from a batch containing 125 g of resin. The dispersing agent and VGCNFs were added as dictated by the design, and initially blended with the resin by hand. Then, batches of VGCNF/resin were mixed using a high-shear mixer (Model L4RT-A, Silverson Machines, Inc., East Longmeadow, MA) at 4500 rpm and/or an ultrasonic processor (Model GEX750-5C, GENEQ, Inc., Montreal, Canada) operating at a continuous power amplitude of 20%. For design

Table II. Average Normalized Impact Strength Values by Configuration

Experimental run no.	x_1	x_2	x_3	Freq.[a]	S/S_{VE}[b]	Std. Dev.
1	0	$-\sqrt{2}$	0	6	0.889	0.141
2	−1	−1	−1	8	0.906	0.139
3	1	−1	−1	8	0.822	0.082
4	−1	−1	1	7	0.899	0.138
5	1	−1	1	6	0.928	0.196
6	0	0	$-\sqrt{2}$	6	0.907	0.228
7[c]	$-\sqrt{2}$	0	0	6	1.050	0.076
8	$\sqrt{2}$	0	0	7	0.910	0.173
9	0	0	$\sqrt{2}$	7	0.841	0.231
10	−1	1	−1	6	1.020	0.160
11	1	1	−1	7	0.926	0.189
12	−1	1	1	6	0.955	0.258
13	1	1	1	7	1.010	0.179
14	0	$\sqrt{2}$	0	7	0.927	0.237
15[c]	0	0	0	7	0.807	0.158
16	0	0	0	7	0.862	0.154
17	0	0	0	7	0.850	0.219
18	0	0	0	7	0.812	0.150

[a]Number of tests in each experimental run, [b]Normalized impact strength, [c]Experimental runs used for scanning electron micrographs.

Table III. VGCNF/VE Materials Formulation

Ingredient	Weight (g)
Derakane 441-400 (VE resin)	100
Cobalt naphthenate 6 wt % (promoter)	0.200
BYK-A 515 (air release agent)	0.200
BYK-A 555 (air release agent)	0.200
BYK-9076 (dispersing agent)	1: 1 with respect to VGCNF
Vapor-grown carbon nanofiber (VGCNF)	0.176/0.300/ 0.600/0.900/1.024
Methyl ethyl ketone peroxide (initiator)	1.000

points utilizing both mixing methods, high-shear mixing was always performed prior to ultrasonication. The mixing times corresponded to the CCD design points discussed previously. To prevent resin heating during processing, the container holding the resin mixture was placed in an ice bath for the full duration of high-shear mixing. Ice bath immersion was also used for ultrasonication times longer than $X_3 = 8.79$ min. The polymerization initiator (MEKP) was added last and hand-stirred for several minutes. The mixture was placed under vacuum and degassed until no more air bubbles visibly rose to the resin surface. Lastly, the mixture was carefully poured into the specimen mold and placed in a preheated oven (Fisher Scientific, Pittsburgh, PA) for curing. The nanocomposite specimens were cured in a nitrogen atmosphere for 5 h at 60°C and then post-cured for 2 h at 120°C, similar to the curing protocol followed by Nouranian et al.[10] and Lee.[12]

Pretest Specimen Preparation

Fabricated nanocomposite specimens were sanded to remove surface imperfections prior to testing. In particular, any remaining air bubbles in the liquid resin mixture that formed air pockets in the cured specimens along the open face of the mold were removed. A water sander was used to polish the nanocomposite specimens to reduce the heating due to friction during sanding. After polishing, the width and depth of the specimens were measured at three different locations along the specimen length to ensure that they adhered to ASTM D256[35] standard dimensions (Figure 2). All specimens were notched to a depth of 54 mm using a notch cutter (Testing Machines, Inc., Ronkonkoma, NY) in accordance with ASTM D256.

Testing Procedure and Characterization

The impact strengths (a measure of the energy absorbed during dynamic fracture) of VGCNF/VE nanocomposites were measured by standard notched Izod impact testing conducted at room temperature. A pendulum style impact tester (Testing Machines, Inc., Ronkonkoma, NY) equipped with a 0.454 kg Izod hammer was employed in accordance with ASTM D256. Before testing the nanocomposite specimens, seven neat VE samples were tested to establish a baseline. Impact strength values were each normalized against the mean impact strength of the neat VE ($S_{VE} = 17.142$ J/m). A total of 122 nanocomposite specimens were tested with a minimum of six specimens for each experimental run (Table II).

The fracture surfaces of four specimens were analyzed using a JEOL field emission scanning electron microscope (SEM) at a power of 5 kV to determine the nanocomposite physical characteristics (i.e., nanofiber dispersion, void formation, etc.) that affect the impact strength. One specimen with the highest measured impact strength among the six axial design point specimens in run no. 7 (Table II), and two specimens with the lowest and highest measured impact strengths from the design center point in run no. 15 (Table II) were selected. The axial design point ($X_1 = 0.176$ phr, $X_2 = 50$ min, and $X_3 = 30$ min; run no. 7) was chosen, because it had the highest mean normalized impact strength ($S/S_{VE} = 1.050$). The specimen with the highest measured strength from this run had a normalized impact strength $S/S_{VE} = 1.118$. The center point run ($X_1 = 0.600$ phr, $X_2 = 50$ min, and $X_3 = 30$ min; run no. 15) had the lowest average normalized impact strength ($S/S_{VE} = 0.807$) of the four center point runs. The specimens with the lowest and highest measured strength from this run had normalized impact strength values $S/S_{VE} = 0.579$ and 1.059, respectively. These specimens were chosen to assess the physical attributes leading to lower impact strengths at a higher VGCNF weight fraction ($X_1 = 0.600$ phr) prepared with the same mixing times as the axial design point ($X_1 = 0.176$ phr).

RESULTS AND DISCUSSION

Analysis of Variance (ANOVA)

The statistical analysis software, SAS® 9.2, was used to generate the ANOVA table and perform the regression analysis for the nanocomposite impact strengths. Initially, the full second-order coded model [eq. (3)] was fit to the data. The ANOVA table for the second-order coded model is given in Table IV. The significance of each regression parameter estimate was checked in

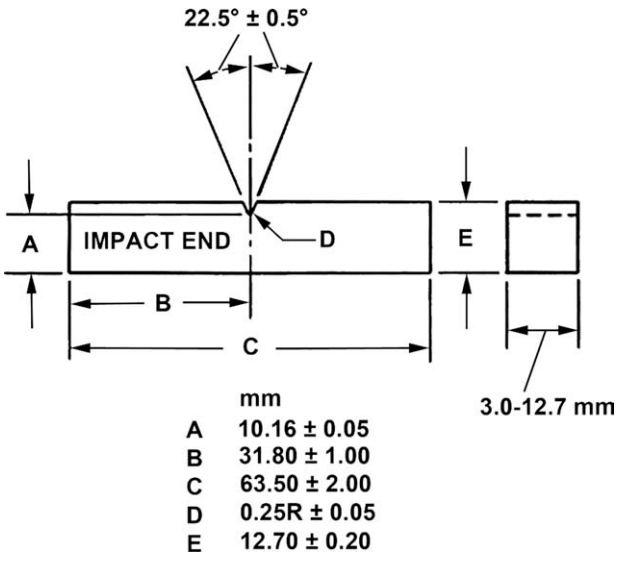

Figure 2. Dimensions of notched Izod impact specimens (Adapted from Ref. 35).

Table IV. Full Second-Order Coded Model ANOVA Table

Source	DoF[a]	Sum of squares	Mean square	*F*-value	*P*-value
Model	9	0.06984	0.00776	4.40	0.0243[b]
Error	8	0.01410	0.00176	-	-
Lack of fit	5	0.01187	0.00237	3.19	0.1841
Pure error	3	0.00223	0.00074	-	-
Corrected total	17	0.08394	-	-	-

	$R^2 = 0.8320$		Adjusted $R^2 = 0.6430$		
Parameter	DoF[a]	Parameter estimate	Standard error	*t*-Value	*P*-value
b_0	1	0.83963	0.01979	442.00	<0.0001[b]
b_1	1	-0.02478	0.01212	-2.04	0.0751[b]
b_2	1	0.03416	0.01212	82.00	0.0225[b]
b_3	1	0.00174	0.01212	0.14	0.8897
b_{12}	1	0.00137	0.01484	0.09	0.9288
b_{13}	1	0.03295	0.01484	22.00	0.0572[b]
b_{23}	1	-0.01060	0.01484	-0.71	0.4955
b_{11}	1	0.06333	0.01485	4.27	0.0027[b]
b_{22}	1	0.02717	0.01485	1.83	0.1046
b_{33}	1	0.01026	0.01485	0.69	0.5090

[a]Degrees of freedom, [b]Significant *P*-values (<0.1).

order to remove terms that were not contributing to the impact strength predictions in the full quadratic form of the RSM. The *P*-value for each parameter estimate, which is based on a partial *t*-test, is an indicator of a term's contribution to the predicted response if that term enters the model last and all other terms are already in the model.[34] Typically, a parameter estimate having a *P*-value less than 0.05 would indicate that this parameter made a significant contribution to the predicted response and the parameter estimate would be retained in the model. However, in this analysis, all parameter estimates with an initial *P*-value $\leq$ 0.1 were kept in the model. This ensures that significant terms are not prematurely removed from the full model due to error introduced by parameter estimates with extremely high *P*-values. An example of such a parameter is b_{12} (*P*-value = 0.9288), which corresponds to the interaction $x_1 \times x_2$.

The full second-order model was significant since its *P*-value (0.0243, Table IV) was less than the maximum threshold *P*-value (0.05). An alternative statistical measure of how well the model approximated the test results is the lack of fit *P*-value.[34] Unlike the model *P*-value, it is desirable for the lack of fit *P*-value to exceed a threshold value of 0.05. The full second-order model's lack of fit *P*-value (0.1841, Table IV) exceeded the minimum threshold value for significance. Hence, the full second-order model was statistically significant, but since several parameter estimates were insignificant, a statistically improved reduced model was developed.

The reduced model (Table V) included all of the parameter estimates determined to be significant in the full second-order model and their corresponding factor(s) denoted by an asterisk in Table IV. If an interaction term is significant and included in the RSM, then all lower order terms completely contained in the higher order term must also be retained in the RSM; this corresponds to the principle of hierarchy.[23] Hence, the regression parameter estimate b_3 corresponding to the coded ultrasonication time (x_3) was also included in the reduced model because the $x_1 \times x_3$ interaction term was significant.

The ANOVA (Table V) indicated that the reduced model was more representative of the significantly contributing variable interactions than the full second-order model (Table IV). The *P*-values for the parameter estimates were indicators of the reduced model's adequacy. All of the *P*-values were less than 0.05 except for those corresponding to the estimates for b_3 and b_{22}. The x_3 term must be kept in the model due to hierarchy as previously discussed. The *P*-value for the b_{22} parameter estimate was slightly larger than the 0.05 level of significance traditionally used for RSMs.[26,32] If b_{22} were removed from the model, however, the R^2-value and adjusted R^2-values (measures of the amount of variability in the data that can be explained by the model) would drop substantially. Unlike the R^2-value, which will always increase as terms are added to a model, the adjusted R^2-value is penalized in a way that it will decrease if unnecessary terms are added to the model. For example, the full second-order model has an R^2-value of 0.8320 (Table IV) compared to an R^2-value of 0.8111 for the reduced model (Table V). Slightly more variation could be explained by the second-order model with more terms in it, but by comparing the adjusted R^2-values of the full second-order model (0.6430) with the reduced model (0.7079), the reduced model explained more variance with fewer terms.

Table V. Reduced Coded Model ANOVA Table

Source	DoF[a]	Sum of squares	Mean square	*F*-value	*P*-value
Model	6	0.06808	0.01135	7.87	0.0018[b]
Error	11	0.01586	0.00144	-	-
Lack of fit	8	0.01363	0.00170	29.00	0.2671
Pure error	3	0.00223	0.00074	-	-
Corrected total	17	0.08394	-	-	-

	$R^2 = 0.8111$		Adjusted $R^2 = 0.7079$		
Parameter	DoF[a]	Parameter estimate	Standard error	*t*-Value	*P*-value
b_0	1	0.84647	0.01550	54.61	<0.0001[b]
b_1	1	-0.02478	0.01096	-26.00	0.0450[b]
b_2	1	0.03416	0.01096	3.12	0.0098[b]
b_3	1	0.00174	0.01096	0.16	0.8771
b_{13}	1	0.03295	0.01342	45.00	0.0320[b]
b_{11}	1	0.06333	0.01343	4.72	0.0006[b]
b_{22}	1	0.02718	0.01343	2.02	0.0680

[a]Degrees of freedom, [b]Significant *P*-values (<0.05).

Response Surface Model (RSM)

The reduced fitted RSM for estimating impact strengths is given in its coded form as

$$\frac{\widehat{S}}{S_{VE}} = 0.84647 - 0.024784x_1 + 0.03416x_2 + 0.00174x_3 + \\ + 0.03295x_1x_3 + 0.06333x_1^2 + 0.02718x_2^2 \quad (4)$$

where parameter estimates from Table V have been included in the model. The RSM can be transformed to its uncoded form using eq. (1), that is,

$$\frac{\widehat{S}}{S_{VE}} = 1.24626 - 1.08285X_1 - 0.00121X_2 - 0.00303X_3 + \\ + 0.00518X_1X_3 + 0.70406X_1^2 + 0.00172X_2^2 \quad (5)$$

The uncoded RSM was used to predict normalized impact strengths as a function of VGCNF weight fraction (X_1), high-shear mixing time (X_2), and ultrasonication time (X_3). Figure 3 shows the predicted impact strengths ($\widehat{S}/S_{VE}$) as a function of VGCNF weight fraction (X_1 = 0.176–1.024 phr) at high-shear mixing times X_2 = 0, 50, and 100 min. The ultrasonication time was held constant at X_3 = 0, 30, and 60 min in Figure 3(a–c), respectively. Examination of Figure 3(a) revealed that an increase in impact strengths was possible at low VGCNF weight fractions. The greatest predicted impact strength increase ($\widehat{S}/S_{VE}$ = 1.180) occurred for a nanocomposite fabricated using the minimum VGCNF weight fraction (X_1 = 0.176 phr; $x_1 = -\sqrt{2}$) and the maximum high-shear mixing time (X_2 = 100 min; $x_2 = \sqrt{2}$). In general, nanocomposites prepared using the maximum high-shear mixing time (X_2 = 100 min) demonstrated the greatest relative improvement in predicted impact strengths over a larger range of VGCNF weight fractions (X_1 < 0.450 phr) when compared to nanocomposites prepared using the high-shear mixing times X_2 = 0 and 50 min. As the VGCNF weight fraction was further increased (X_1 > 0.450 phr), all of the predicted strengths fell below those of the neat VE (i.e., $\widehat{S}/S_{VE}$ < 1.0). It should also be noted that the curves for X_2 = 0 and 50 min were nearly coincident, suggesting that there was no significant benefit gained from high-shear mixing times X_2 < 50 min.

The preceding results were obtained for nanocomposites prepared without ultrasonication (X_3 = 0 min; $x_3 = -\sqrt{2}$). For low VGCNF weight fractions (X_1 < 0.450 phr), the predicted impact strengths decreased with increasing ultrasonication times (X_3) [Figure 3(b,c)]. Interestingly, at higher nanofiber weight fractions (X_1 > 0.850 phr) modest improvements in predicted impact strengths were obtained as both the high-shear mixing and ultrasonication times were maximized (X_2 = 100 min, X_3 = 60 min; $x_2 = x_3 = \sqrt{2}$).

Figure 4 contains plots of the predicted normalized impact strengths ($\widehat{S}/S_{VE}$) as a function of VGCNF weight fraction (X_1) for the ultrasonication times X_3 = 0, 30, and 60 min. The high-shear mixing time was held constant at X_2 = 0, 50, and 100 min for plots 4(a–c), respectively. At low VGCNF weight fractions, (X_1 < 0.3 phr), the predicted impact strengths decreased with increasing ultrasonication times [Figure 4(a)]. After reaching a local minimum at weight fractions in the range of 0.040 ≤ X_1 ≤ 0.080 phr, the impact strengths increased with both increasing VGCNF weight fraction and ultrasonication time. The predicted impact strengths, however, fell below that of the neat VE (i.e., $\widehat{S}/S_{VE}$ < 1.0). A comparison of Figure 4(a–c) suggests that increasing the duration of high-shear mixing results in a notable improvement in impact strengths over the entire range of VGCNF weight fractions and ultrasonication times. There are several possible explanations for the observed behavior. Extended high-shear mixing time is likely very effective in

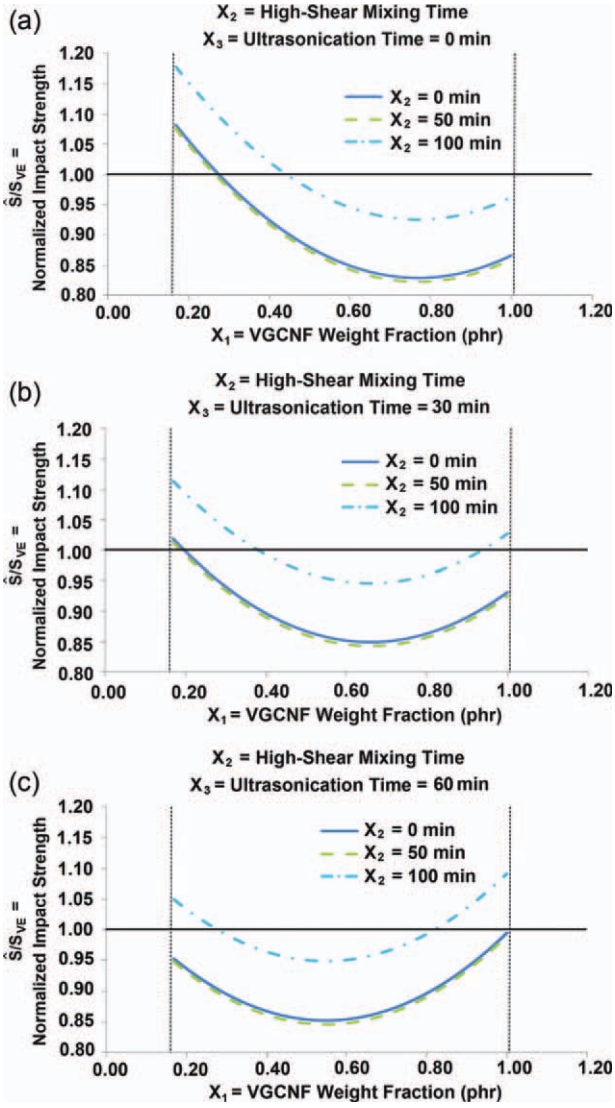

Figure 3. Effects of high-shear mixing time (X_2), at constant ultrasonication time (X_3), on predicted impact strength ($\widehat{S}/S_{VE}$) as a function of VCGNF weight fraction (X_1) at (a) $X_3 = 0$ min, (b) $X_3 = 30$ min, and (c) $X_3 = 60$ min. [Color figure can be viewed in the online issue, which is available at wileyonlinelibrary.com]

distributing loose nanofibers in the liquid resin, as well as breaking up large VGCNF agglomerates into smaller nests. After high-shear mixing, the largest agglomerate size may be dictated by high-shear mixer's screen size. Ultrasonication is likely less effective in dispersing the VGCNFs at low volume fractions without significant styrene evaporation. This may explain why high-shear mixing leads to better predicted strengths at low VGCNF weight fractions. At higher nanofiber weight fractions, however, the proportionally larger number of intermediate-sized agglomerates remaining after high-shear mixing may result in lower impact strengths. Extended ultrasonication may serve to break up a fraction of these nests, resulting in a modest relative increase in impact strengths at higher weight fractions.

Finally, the fitted RSM was used to predict normalized impact strengths ($\widehat{S}/S_{VE}$) as a continuous function of high-shear mixing time (X_2) at ultrasonication times $X_3 = 0$, 30, and 60 min (i.e., $x_3 = -\sqrt{2}$, 0, $\sqrt{2}$; Figure 5). The VGCNF weight fraction was fixed at $X_1 = 0.176$, 0.600, and 1.024 phr ($x_1 = -\sqrt{2}$, 0, $\sqrt{2}$) in Figure 5(a–c), respectively. For composites containing the lowest amount of VGCNFs ($X_1 = 0.176$ phr), the optimal impact strengths occurred with increased high-shear mixing and no ultrasonication ($X_3 = 0$ min). Increased ultrasonication times led to a decrease in estimated impact strengths [Figure 5(a)]. As the amount of VGCNFs increased to an intermediate level [$X_1 = 0.600$ phr, Figure 5(b)], no combination of mixing times led to an improvement in impact strengths and the estimated impact strengths all fell below that of the neat VE ($\widehat{S}/S_{VE} < 1.0$). As the weight fraction of nanofibers was maximized [$X_1 = 1.024$ phr, Figure 5(c)], however, a modest improvement in the predicted strengths occurred in composites prepared using the maximum high-shear mixing and ultrasonication times ($X_2 =$

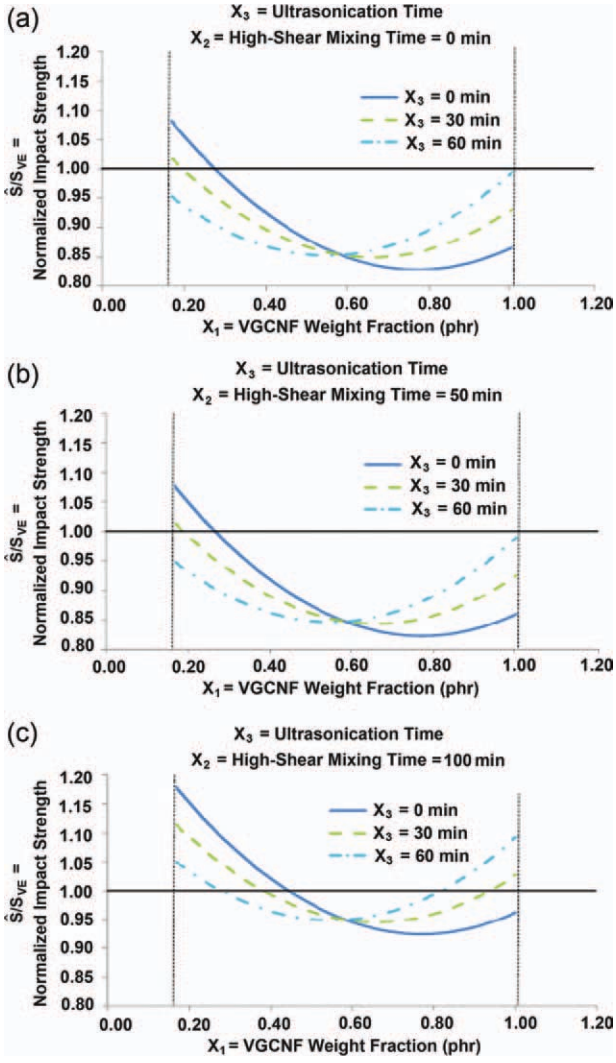

Figure 4. Effects of ultrasonication time (X_3), at constant high-shear mixing time (X_2), on predicted impact strength ($\widehat{S}/S_{VE}$) as a function of VCGNF weight fraction (X_1) at (a) $X_2 = 0$ min, (b) $X_2 = 50$ min, and (c) $X_2 = 100$ min. [Color figure can be viewed in the online issue, which is available at wileyonlinelibrary.com]

Applied Polymer SCIENCE

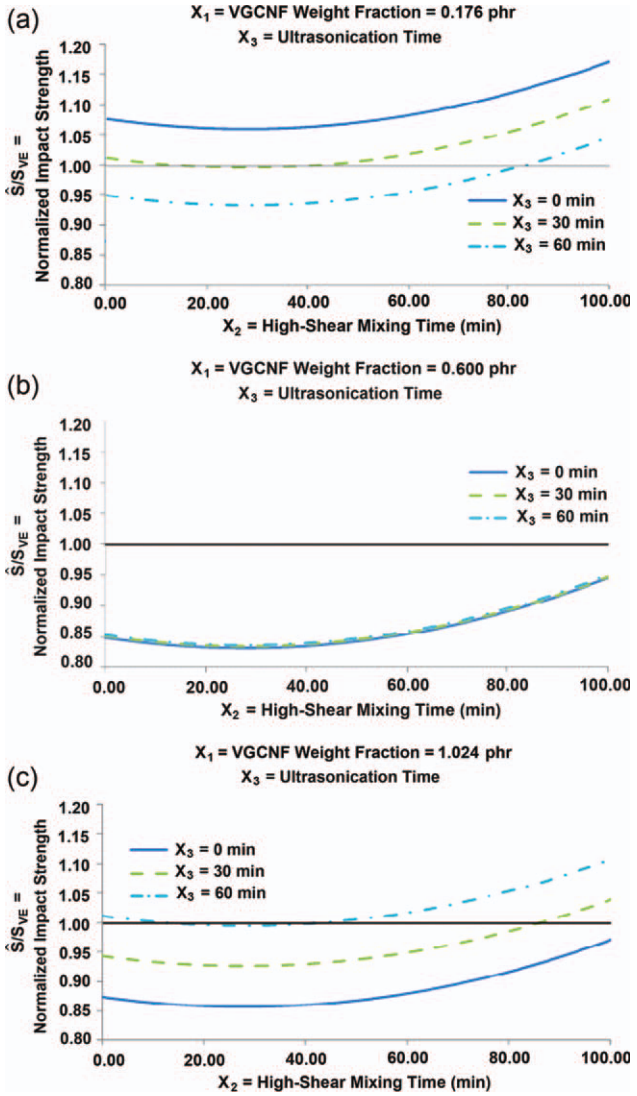

Figure 5. Effects of ultrasonication time (X_3), at constant VGCNF weight fraction (X_1), on predicted impact strength ($\widehat{S}/S_{VE}$) as a function of high-shear mixing time (X_2) at (a) X_1= 0.176 phr, (b) X_1 = 0.600 phr, and (c) X_1 = 1.024 phr. [Color figure can be viewed in the online issue, which is available at wileyonlinelibrary.com]

100 min, X_3 = 60 min). As an aside, the predicted impact strengths clearly increase with increasing high-shear mixing times (Figure 5). This suggests that nanofiber chopping does not have a detrimental effect on composite strengths for the mixing times considered in this study. These observations are consistent with predictions by Yu et al.,[8,36,37] indicating that a significant degradation in VGCNF/VE nanocomposite elastic moduli only occurs when the degree of nanofiber chopping is fairly severe ($L/D < 90$).

Note that the RSM developed in this study can easily be used to sort out the complex interactions between material and fabrication parameters that lead to relative improvements in nanocomposite properties. This would have been impossible using traditional single-variable experimental approaches. As an aside, the given RSM predicts that a minor improvement in properties is possible for composites containing small amounts of carbon nanofibers (X_1 = 0.176 phr) and prepared using no mixing [X_2 = X_3 = 0 min, Figure 5(a)]. Clearly, such a result is not physical and likely is a consequence of using a second-order regression model. Similarly, the predicted results suggest that slight relative enhancements in strength are possible at higher VGCNF weight fractions [Figure 3(b,c)]. In practice, further increases in the amount of nanofibers would likely result in a decrease in impact strengths due to poor nanofiber dispersion. Nanocomposites containing higher VGCNF weight fractions cannot be reasonably processed via the sonication and mixing techniques used in this work due to dramatic increases in liquid resin viscosity with increasing amounts of VGCNFs. Three-roll milling is required to get acceptable nanodispersion at higher VGCNF weight fractions. Good dispersion of nanofibers is crucial in order to maximize properties. The RSM developed here can be used to sort out the optimal combination of independent variables that lead to the highest impact strengths.

SEM Imaging of Fracture Surfaces

SEM observations were made near the fracture initiation site (machined notch root) of nanocomposite specimens prepared using fixed mixing times (X_2 = 50 min, X_3 = 30 min; x_2 = x_3 = 0), but with varying VGCNF amounts (X_1 = 0.176 and 0.600 phr; x_1 = $-\sqrt{2}$ and 0). Figure 6(a–c) contains low magnification SEM images of the fracture surfaces for an axial design point specimen (X_1 = 0.176 phr; highest measured normalized impact strength, S/S_{VE} = 1.118), the highest strength center point specimen (X_1 = 0.600 phr; measured S/S_{VE} = 1.059), and the lowest strength center point specimen (X_1 = 0.600 phr; measured S/S_{VE} = 0.579), respectively. Both high-strength specimens [Figure 6(a,b)] displayed rough fracture surfaces consistent with higher fracture toughness values. In contrast, the fracture surface of the lowest strength center point specimen (measured S/S_{VE} = 0.579) is clearly smoother [Figure 6(c)], indicative of cleavage fracture typical of lower strength, brittle materials with unstable crack growth. Poor VGCNF dispersion or the presence of stress risers, such as the two VGCNF agglomerates evident in Figure 6(c), can dramatically reduce the impact strength of the nanocomposite. The larger agglomerate is ~80 μm across with a distinct crack emanating from it in the fracture direction. Likewise, the smaller agglomerate (~25 μm across) also appears to have served as a crack initiation site.

Figure 7(a,b) contains higher magnification SEM images of the fracture surfaces for the high-strength and low-strength center point specimens shown in Figure 6(b,c), respectively. In Figure 7(a), well-dispersed nanofibers (exposed nanofiber ends, nanofiber pull-out holes, and nanofiber imprints) are evident throughout the polymer matrix. Well-dispersed nanofibers may mitigate crack growth and enhance strength by bridging the crack opening at the onset of fracture initiation. In contrast, Figure 7(b) contains an image of a large bundle of unwetted nanofibers imaged near the leading edge of the large agglomerate shown in Figure 6(c). The large carbon nanofiber bundle provides a stress concentration location that may facilitate localized crack initiation leading to global fracture. Also, the unwetted nanofibers contained in VGCNF agglomerates were not

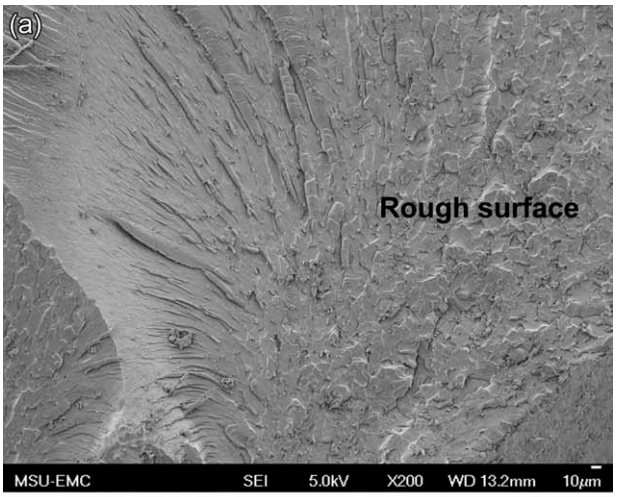

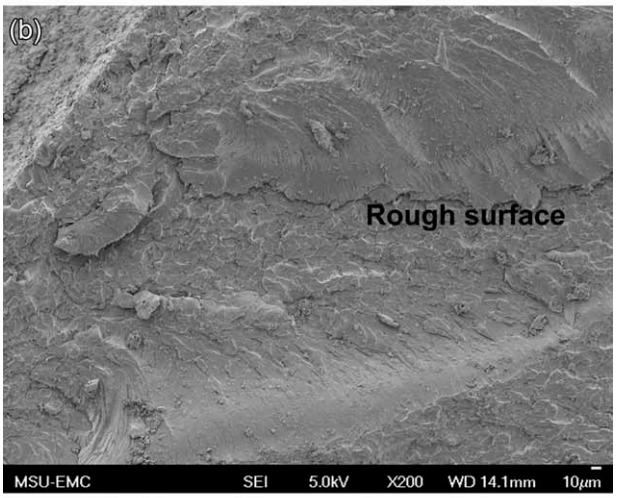

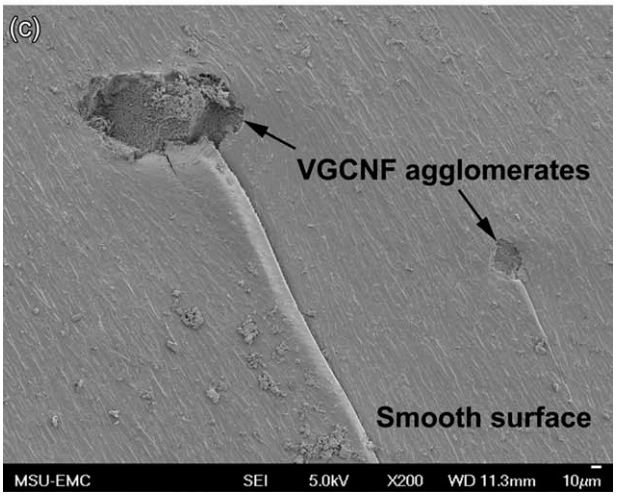

Figure 6. Low magnification SEM images of representative fracture surfaces within 1 mm of the fracture initiation site for specimens prepared using high-shear mixing time (X_2 = 50 min) and ultrasonication time (X_3 = 30 min). (a) Axial design point specimen (VGCNF weight fraction X_1 = 0.176 phr) with the highest measured impact strength (S/S_{VE} = 1.118). (b) Center point specimen (X_1 = 0.600 phr) with the highest measured impact strength (S/S_{VE} = 1.059). (c) Center point specimen (X_1 = 0.600 phr) with the lowest measured impact strength (S/S_{VE} = 0.579).

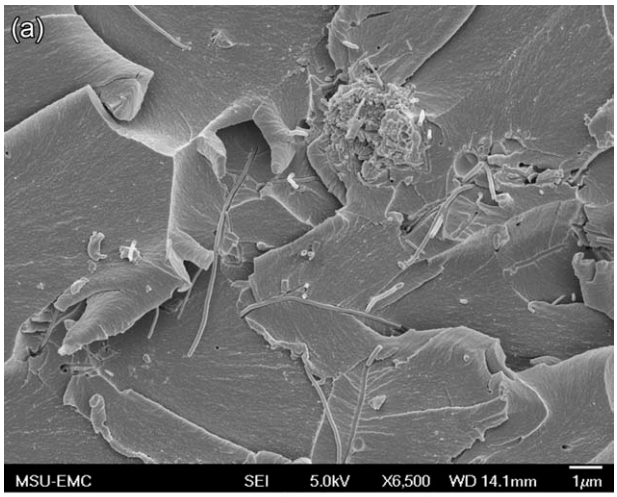

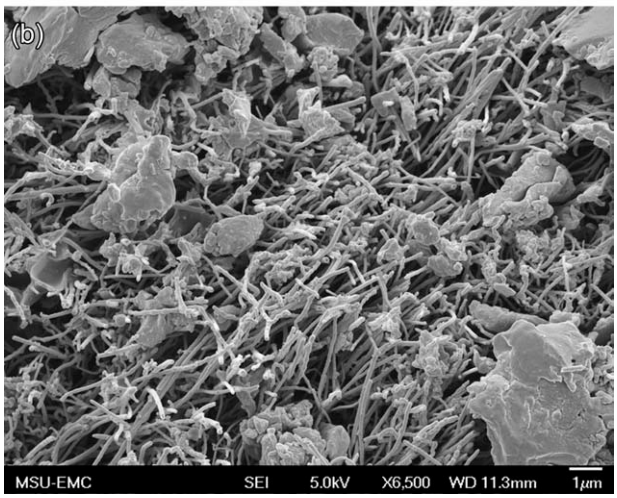

Figure 7. High magnification SEM images of representative fracture surfaces within 1 mm of the fracture initiation site for center point specimens. (a) Dispersed fibers near the fracture initiation site ($\leq$ 1 mm) for the specimen with the highest measured strength (S/S_{VE} = 1.059). (b) Unwetted fiber bundle near the fracture initiation site ($\leq$ 1 mm) for the specimen with the lowest measured strength (S/S_{VE} = 0.579).

available to mitigate fracture elsewhere in the specimen. This lead to a further reduction in the local crack opening resistance.

The carbon nanofibers in specimens with a VGCNF weight fraction X_1 = 0.176 phr were generally more uniformly dispersed than those with a VGCNF weight fraction X_1 = 0.600 phr. At lower VGCNF weight fractions, increased high-shear mixing was better able to efficiently disperse the carbon nanofibers because the uncured VGCNF/VE blend had a relatively low viscosity. At higher VGCNF weight fractions with increased resin viscosity, high-shear mixing was less effective in mechanically dispersing the VGCNFs. This is potentially due to less uniform stirring of the more viscous resin mixture via the high-shear mixing head. The SEM images show that good nanofiber dispersion is possible for a portion of the nanofibers at a VGCNF weight fraction X_1 = 0.600 phr [Figure 7(a)], but large agglomerates are also present [Figure 6(c)]. This may lead to nanocomposites with relatively high moduli, but poor strengths.

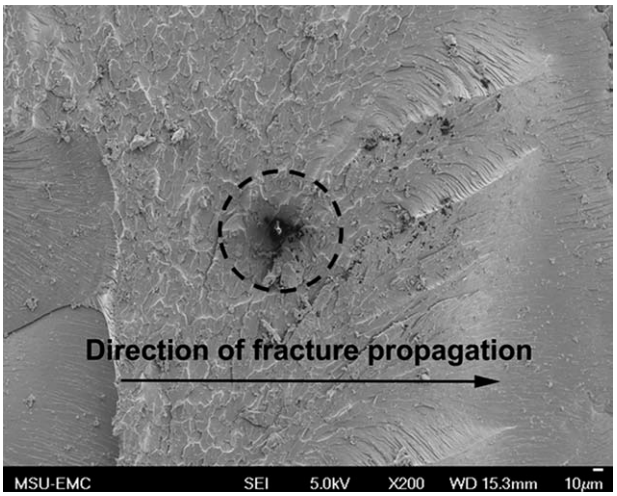

Figure 8. Low magnification SEM image illustrating the transition from a rough to smooth fracture surface for an axial design point specimen (VGCNF weight fraction $X_1 = 0.176$ phr; high-shear mixing time $X_2 = 50$ min; ultrasonication time $X_3 = 30$ min) with the highest measured impact strength ($S/S_{VE} = 1.118$).

The SEM images in Figures 6 and 7 were taken within 1 mm of the fracture initiation site (notch root). Figure 8 contains an image that was captured at a distance between 1.5 and 2 mm from the fracture initiation site. The appearance of the fracture surface transitions from rough to smooth with increasing crack propagation shown moving from left to right in Figure 8. This indicates that the carbon nanofibers likely only inhibit crack growth for relatively small cracks. Once the crack exceeds a certain size, the nanofibers no longer provide a significant resistance to crack extension.

Multiple voids are also evident in Figure 8. The largest void (circled) is ~30–40 μm in diameter (about 1/8th the length of the longest VGCNF). Voids may result from air bubbles entrapped in the liquid resin during processing or may nucleate during the fracture event. Similar to agglomerates, processing-induced voids cause stress concentrations in the surrounding material that can lead to accelerated localized crack growth. Such voids are likely an unavoidable by-product of the manufacturing techniques.

SUMMARY AND CONCLUSIONS

A CCD was employed to investigate the effects of VGCNF weight fraction, high-shear mixing time, and ultrasonication time on VGCNF/VE nanocomposite impact strengths. A full quadratic RSM was fit to the normalized impact strength data and analyzed using ANOVA. The fitted reduced RSM, determined from the ANOVA results, was employed to predict VGCNF/VE nanocomposite impact strengths within the design space of the experiments.

Based upon RSM predictions, nanocomposites processed with the maximum high-shear mixing time ($X_2 = 100$ min) and no ultrasonication, showed predicted impact strength improvements ($\widehat{S}/S_{VE} > 1$) with VGCNF weight fractions $X_1 < 0.450$ phr. A reduction in predicted impact strength ($\widehat{S}/S_{VE} < 1$) occurred in nanocomposites prepared with VGCNF weight fractions $X_1 = 0.450$–0.800 phr regardless of the mixing regimen. Therefore, it is advisable to use low VGCNF weight fractions and mix the nanocomposite components using only high-shear mixing. However, if the nanocomposite is being used in an application requiring higher carbon nanofiber weight fractions (i.e., for electrical/thermal conductivity), ultrasonication may be used to improve nanofiber dispersion and maintain higher impact strengths. For this study, the optimal mixing protocol for low VGCNF weight fractions was high-shear mixing time $X_2 = 100$ min and ultrasonication time $X_3 = 0$ min. Using optimal mixing, an 18% increase in impact strength was predicted with $X_1 = 0.170$ phr VGCNFs before dropping below the impact strength of neat VE at $X_1 = 0.450$ phr VGCNFs. It seems remarkable that this tiny amount of carbon nanofibers (~0.1 v%) could produce such a marked impact strength improvement.

The design of experiments methodology led to the determination of various nonintuitive formulation and processing factor interactions, such as the interaction between ultrasonication and VGCNF weight fraction, which would have been impossible using traditional single variable test methods. By understanding such complex interactions, nanocomposite formulations can be tailored to optimize or maintain the nanocomposite impact strength while maximizing other properties.

ACKNOWLEDGMENTS

This work was sponsored by the U. S. Department of Energy under contract DE-FC26-06NT42755. Special thanks go to William Joost, Department of Energy's technology area development manager.

REFERENCES

1. Hussain, F.; Hojjati, M.; Okamoto, M.; Gorga, R. E. *J. Compos. Mater.* **2006,** *40*, 1511.
2. Ray, S. S.; Bandyopadhyay, J.; Bousmina, M. *Polym. Degrad. Stab.* **2007,** *92*, 802.
3. Chiu, Y. C.; Ma, C. C. M.; Liu, F. Y.; Chiang, C. L.; Riang, L.; Yang, J. C. *Eur. Polym. J.* **2008,** *44*, 1003.
4. Shariffudin, S.; Mamat, M.; Rusop, M.; Jumali, N.; Shaameri, Z.; Hamzah, A. Proceedings of the International Conference on Electronic Devices, Systems and Applications (ICEDSA), IEEE Publishing; Kuala Lumpur, Malaysia, **2010,** p 380.
5. Mittal, V. Optimization of Polymer Nanocomposite Properties; Wiley-VCH: Weinheim, Germany, **2010.**
6. Schmidt, G.; Malwitz, M. M. *Curr. Opin. Colloid Interface Sci.* **2003,** *8*, 103.
7. Tibbetts, G. G.; Lake, M. L.; Strong, K. L.; Rice, B. P. *Compos. Sci. Technol.* **2007,** *67*, 1709.
8. Yu, J.; Lacy, T. E.; Toghiani, H.; Pittman, C. U., Jr.; Schneider, J. *J. Compos. Mater.* **2011.** DOI: 10.1177/0021998311428361.
9. Jordan, J.; Jacob, K. I.; Tannenbaum, R.; Sharaf, M. A.; Jasiuk, I. *Mater. Sci. Eng. A* **2005,** *393*, 1.
10. Nouranian, S.; Toghiani, H.; Lacy, T. E.; Pittman, C. U.; Dubien, J. *J. Compos. Mater.* **2011,** *45*, 1647.

11. Nouranian, S.; Toghiani, H.; Lacy, T.; Pittman C, Jr. Proceedings of SAMPE Symposium and Exhibition, SAMPE Publishing, SAMPE'09; Baltimore, MD, **2009.**
12. Lee, J. The effect of material and processing on the mechanical response of vapor-grown carbon nanofiber/vinyl ester nanocomposites. M.S. Thesis, Mississippi State University, Mississippi State, MS, **2010.**
13. Green, K. J.; Dean, D. R.; Vaidya, U. K.; Nyairo, E. *Compos. Appl. Sci. Manuf.* **2009,** *40*, 1470.
14. Petrek, C. M.; Garea, S. A.; Iovu, H. *Mat. Plast.* **2008,** *45*, 34.
15. Zhong, W. H.; Li, J.; Xu, L. R.; Michel, J. A.; Sullivan, L. M.; Lukehart, C. M. *J. Nanosci. Nanotechnol.* **2004,** *4*, 794.
16. Zhamu, A.; Wingert, M.; Jana, S.; Zhong, W. H.; Stone, J. J. *Compos. Appl. Sci. Manuf.* **2007,** *38*, 699.
17. Jimenez, G. A.; Jana, S. C. *Carbon* **2007,** *45*, 2079.
18. Nouranian, S.; Jang, C.; Lacy, T. E.; Gwaltney, S. R.; Toghiani, H.; Pittman C. U., Jr. *Carbon* **2011,** *49*, 3219.
19. Jang, C.; Nouranian, S.; Lacy, T. E.; Gwaltney, S. R.; Toghiani, H.; Pittman C. U., Jr. *Carbon* **2012,** *50*, 748.
20. Fidelus, J.; Wiesel, E.; Gojny, F.; Schulte, K.; Wagner, H. *Compos. Appl. Sci. Manuf.* **2005,** *36*, 1555.
21. Miyagawa, H.; Drzal, L. T. *Polymer* **2004,** *45*, 5163.
22. Myers, R. H.; Montgomery, D. C.; Anderson-Cook, C. M. Response Surface Methodology: Process and Product Optimization Using Designed Experiments; Wiley: Hoboken, NJ, **2009.**
23. Montgomery, D. C. Design and Analysis of Experiments; Wiley: Hoboken, NJ, **2009.**
24. Rekab, K.; Shaikh, M. Statistical Design of Experiments with Engineering Applications; Taylor & Francis: Boca Raton, FL, **2005.**
25. Lacy, T. E.; Samarah, I. K.; Tomblin, J. S. *SAE Int. J. Aerosp.* **2002,** *1*, 126.
26. Samarah, I. K. Response surface characterization of impact damage and residual strength degradation in composite sandwich panels. Ph.D. Thesis, Wichita State University, Wichita, KS, **2003.**
27. Samarah, I. K.; Weheba, G. S.; Lacy, T. E. *J. Appl. Stat.* **2006,** *33*, 429.
28. Samarah, I. K.; Weheba, G. S.; Lacy, T. E. *SAE Int. J. Aerosp.* **2006,** *1*, 767.
29. Mirmohseni, A.; Zavareh, S. *J. Polym. Res.* **2011,** *18*, 509.
30. Majdzadeh-Ardakani, K.; Navarchian, A. H.; Sadeghi, F. *Carbohydr. Polym.* **2010,** *79*, 547.
31. Joulazadeh, M.; Navarchian, A. H. *Polym. Adv. Technol.* **2010,** *21*, 263.
32. Yalçinkaya, S. E.; Yildiz, N.; Saçak, M.; Çalimli, A. *Turk. J. Chem.* **2010,** *34*, 581.
33. Sudduth, R. D. *Pigment Resin Technol.* **2008,** *37*, 362.
34. Montgomery, D. C.; Runger, G. C. Applied Statistics and Probability for Engineers; Wiley/R. R. Donnelley: Jefferson City, MO, **2010.**
35. ASTM. Standard Test Methods for Determining the Izod Pendulum Impact Resistance of Plastics; ASTM International: West Conshohocken, PA, **2004.**
36. Yu, J.; Lacy T. E., Jr.; Toghiani, H.; Pittman C. U., Jr.; Hwang, Y. *J. Compos. Mater.* **2011,** *45*, 2401.
37. Yu, J.; Lacy, T. E.; Toghiani, H.; Pittman C. U., Jr. *J. Compos. Mater.* **2012**, DOI: 10.1177/0021998312446824.